STRUCTURE DETERMINATION FROM HREM BY CRYSTALLOGRAPHIC IMAGE PROCESSING

Xiaodong Zou and Sven Hovmöller
Structural Chemistry, Arrehnius Laboratory, Stockholm University, SE-106 91 Stockholm, Sweden

Abstract: This chapter demonstrates that it is possible to perform *ab initio* crystal structure determination by HREM. The various steps in a crystal structure determination; recording and quantifying HREM images, analysis and processing of these data to retrieve the projected potential of the crystal and finally determine the atomic coordinates are described.

Key words: HREM, Structure factors, Crystallographic image processing, Contrast transfer function

1. INTRODUCTION

Electron crystallography is an important technique for determination of unknown crystal structures, complementing X-ray and neutron diffraction. The birth of electron crystallography dates back to the discovery that electrons possessed both particle and wave properties. The crystallographers Pinsker, Vainshtein and Zvyagin, solved inorganic crystal structures from electron diffraction patterns, notably texture patterns [1,2,3]. They designed and used their own electron diffraction cameras and quantified electron diffraction intensities and treated them kinematically. In spite of this early start in 1947, electrons have not been used much for crystal structure determination outside Moscow until the last two decades. Unfortunately, the development of electron crystallography for the study of inorganic crystals was long hampered by an exaggerated fear of dynamical effects.

In the early days of high resolution electron microscopy (HREM), some special classes of structures were solved by recognising basic units of a

T.E. Weirich et al. (eds.), Electron Crystallography, 275–300.

projected structure, and determining their arrangement in larger unit cells. The extensive studies of so-called block oxides constituted the beginning of high resolution electron microscopy on inorganic compounds[4]. This meant that a model had to be proposed and verified by comparisons (usually qualitative) with extensive contrast calculations based on dynamical scattering theory. Typically a set of images was calculated, with a range of defocus and crystal thickness values[5]. Structure determination *ab initio* from HREM was not considered to be practicable.

Experience from a number of structure determinations in recent year have proved in practice that unknown crystal structures can be solved from HREM images, irrespective of whether the structures contain light or heavy elements, provided the image is taken from a thin crystal. There is no need to guess the experimental conditions, such as defocus and crystal thickness, since these can be determined experimentally from HREM images. Furthermore, the very important parameters astigmatism and crystal tilt, which in most cases of image simulations have been set to zero although they often cannot be neglected, can also be determined experimentally directly from HREM images. The distortions caused by the above mentioned factors can then largely be compensated for by crystallographic image processing. Random noise can also be eliminated by averaging over many unit cells. The projected crystal symmetry can be determined and imposed exactly to the data. In this way a projected potential map is reconstructed. For structures with one short unit cell axis (≤ 5 Å), atomic coordinates are read out directly from the map, with a precision of 0.2 Ångström or better. For more complex structures, several projections can be merged into a 3D structure. Finally, it is possible to improve the structure model by least squares refinement against accurately quantified SAED data. After refinement, the atoms are typically located within 0.02 Ångström of their correct positions determined from X-ray crystallography.

Here we will demonstrate that it is possible to perform *ab initio* crystal structure determination by HREM. The various steps in a crystal structure determination; recording and quantifying HREM images, analysis and processing of these data to retrieve the projected potential of the crystal and finally determine the atomic coordinates are described.

2. INTERACTIONS BETWEEN ELECTRONS AND MATTER

Electrons interact thousands of times more strongly with matter than X-rays do. This has the advantage that extremely small crystals can be studied, down to a size of a few nanometers in all directions. This is about a million

times smaller than what is needed even for X-ray diffraction using a synchrotron. Many compounds form so small microcrystals that electrons are the only possible source for analysis of their structures.

On the other hand, the strong interaction between electrons and matter gives rise to dynamical effects[13] which complicate quantitative analysis of the experimental data. This has led to a pessimistic view of the possibility of direct crystal structure determination by electron crystallography[14], especially for compounds containing heavy elements. Already after penetrating a few nanometers into the sample, a considerable fraction of the incident beam has been scattered. These scattered electrons may well be scattered again as they propagate through the sample. This multiple scattering results in a diffraction pattern or an image which no longer can be interpreted as a linear function of the structure factor amplitudes or projected crystal potential. It has been widely assumed that this multiple scattering is so severe that not even the thinnest crystals that can be obtained experimentally can be treated as singly scattering (kinematical) objects and that a direct interpretation of HREM images in terms of structure in general would not be possible. Based on this argument, image simulations have been considered necessary for interpretation and validation of suggested structure models.

Plots of amplitudes and phases of the diffracted beams at the exit surface of a crystal calculated by image simulation seem to show rapid changes of both amplitudes and phases with increasing crystal thickness, so that inorganic crystals can not be treated by a simple linear kinematic model if they are thicker than about ten or twenty Ångströms. However, these rapidly changing phases are partly due to the electron wave propagation in the crystal. After the effects of propagation have been removed, phases of the strong diffracted beams are close to the crystallographic structure factor phases, even for crystals thicker than 100Å. Furthermore, the phases obtained from the Fourier transform of the HREM images are not the same as the phases of the diffracted beams at the exit surface of the crystal. The former are affected by the defocus and astigmatism of the objective lens. The relation between the different types of phases, is described by Zou[15]. It has been shown experimentally that the structure factor phases (which are the ones that are needed for a structure determination) can be correctly determined directly from HREM images of relatively thin crystals[10, 15, 16]. This is also supported by theoretical considerations[17,18].

3. CRYSTAL POTENTIAL AND STRUCTURE FACTORS

Electrons are scattered by the electrostatic field generated by the electrostatic potential difference in a crystal. Atoms in a crystal give sharp and positive peaks to the potential. The relation between the potential V(**r**) and the structure factors F(**u**) are

$$V(\boldsymbol{r}) = k\sum_{\boldsymbol{u}} F(\boldsymbol{u}) \exp\left[-2\pi i(\boldsymbol{u}\cdot\boldsymbol{r})\right] \quad (1)$$

where k is a constant. The potential at any point in the crystal can be calculated by adding the vectors $F(\mathbf{u})\exp[-2\pi i(\mathbf{u}\cdot\mathbf{r})]$ for all the structure factors F(**u**), i.e. by Fourier synthesis. In fact, each vector of reflection **u**, together with that of its Friedel mate -**u**, generate a cosine wave[19].

$$F(\mathbf{u})\exp[-2\pi i(\mathbf{u}\cdot\mathbf{r})] + F(-\mathbf{u})\exp[-2\pi i(-\mathbf{u}\cdot\mathbf{r})] = 2|F(\mathbf{u})|\cos[\phi(\mathbf{u})-2\pi(\mathbf{u}\cdot\mathbf{r})] \quad (2)$$

The direction and the periodicity of each cosine wave are given by its index **u** = (*hkl*), the amplitude of the cosine wave is 2|F(**u**)|, proportional to the structure factor amplitude |F(**u**)|. More importantly, the positions of the maxima and minima of the cosine wave (in relation to the unit cell origin) are determined by the structure factor phase $\phi(\mathbf{u})$. If both the amplitudes |F(**u**)| and the phases $\phi(\mathbf{u})$ of the structure factors for all reflections **u** are known, the potential $\varphi(\mathbf{r})$ can be obtained by adding a series of such cosine waves.

An example of this procedure is shown in Fig. 1. This example shows the build-up of the 2D potential of Ti_2S projected along the short *c* axis, but the principle is the same for creating a 3D potential. The potential is a continuous function in real space and can be described in a map (Fig. 1). On the other hand, the structure factors are discrete points in reciprocal space and can be represented by a list of amplitudes and phases (Table 1). In this Fourier synthesis we have used the structure factors calculated from the refined coordinates of Ti_2S[20].

If the Fourier synthesis is carried out by adding in the strong reflections first, we will see how fast the Fourier series converges to the projected potential. The positive potential contribution from the reflection is shown in white, whereas the negative potential contribution is shown in black. Most of the atoms are located in the white regions of each cosine wave, but the exact atomic positions will not become evident until a sufficiently large number of structure factors have been added up.

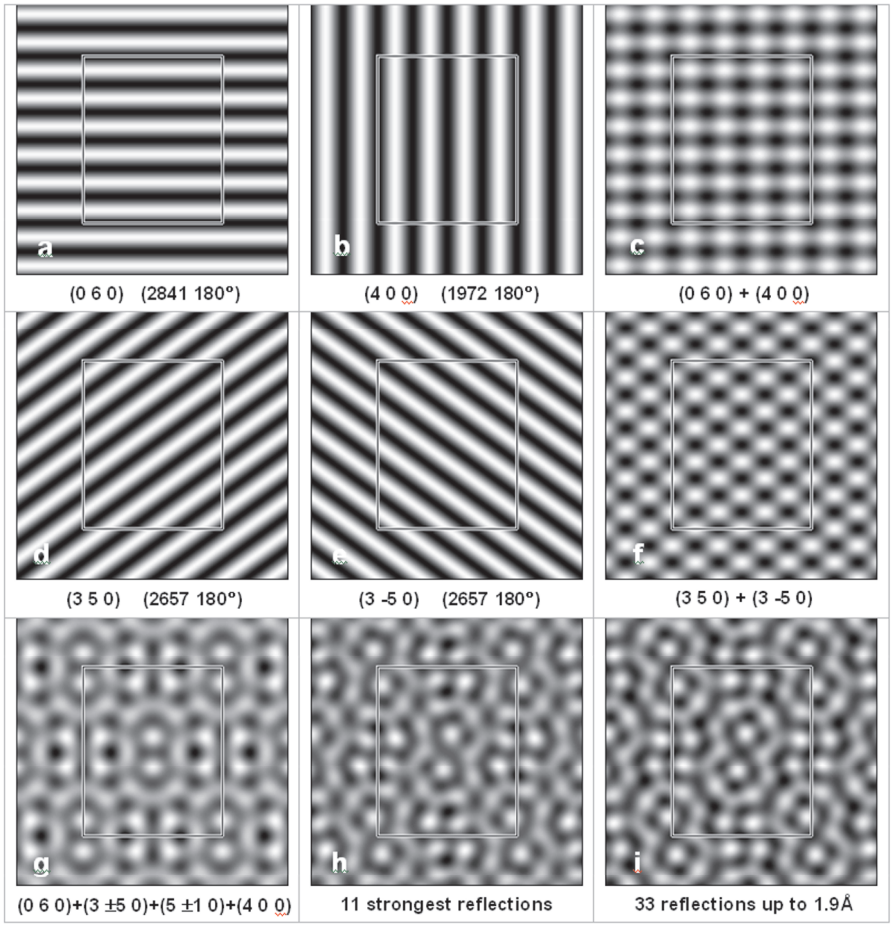

Figure 1 Fourier synthesis of the projected potential map of Ti_2S along the c-axis. Amplitudes and phases of the structure factors are calculated from the refined atomic coordinates of Ti_2S and listed in Table 1. The space group of Ti_2S is *Pnnm* and unit cell parameters a= 11.35, b=14.05 and c=3.32 Å.

Among all the 33 reflections up to 1.6 Å, the strongest one is (0 6 0). This reflection generates a cosine wave which cuts the *a* axis zero times per unit cell and the *b* axis 6 times. It is the phase of each reflection which determines where the maximum and minimum of the cosine wave are. The phase of (0 6 0) is 180^o (Table 1) and thus $\cos 180^o = -1$, the contribution to the potential at the origin is negative (black) (Fig. 1a). Similarly, the cosine wave given by (4 0 0) reflection cuts the *a* axis 4 times and the *b* axis zero times. The phase of (4 0 0) is also 180^o so its contribution to the potential at the origin is also negative (Fig. 1b). The summation of these two cosine waves is shown in Fig. 1c.

Table 1 Amplitudes $F_c(hkl)$ and phases $\phi_F(hkl)$ of all structure factors $F(hkl)$ of Ti_2S with d_{hkl} >1.9Å compared with those obtained from the HREM image. The phases $\phi_{ctf}(hkl)$ listed are after compensation for the CTF and with the origin shifted to the position of the lowest phase residual for *pgg* symmetry. The phases $\phi_{sym}(hkl)$ are the phases after imposing the symmetry. The experimentally determined phases $\phi_{sym}(hkl)$ are virtually identical to the crystallographic structure factor phases $\phi_F(hkl)$; only four (highlighted) out of 33 reflections have wrong phases and all of them are weak reflections.

			Structure factor		Amplitudes and phases from experimental image					
h	k	l	Fc	ϕ_F(hkl)	Amp	ϕ_{AF}(hkl)	ϕ_S(hkl)	Amp	ϕ_{AF}(h-kl)	ϕ_S(h-kl)
0	6	0	2841	180	2706	-133	180	-	0	-
3	5	0	2657	180	2371	174	180	4022	-179	180
5	1	0	2553	0	2609	49	0	3099	2	0
4	0	0	1972	180	1904	140	180	-	-	-
1	7	0	1935	0	613	-10	0	625	19	0
5	2	0	1841	0	1241	-62	0	1553	132	180
5	4	0	1560	0	255	15	0	417	-104	180
4	5	0	1504	180	516	115	180	586	-20	0
4	3	0	1350	0	1674	7	0	2544	-175	180
2	6	0	1308	180	1026	-140	180	1455	180	180
5	3	0	1262	180	530	110	180	642	160	180
4	4	0	1129	180	837	-140	180	1322	133	180
3	6	0	1030	180	274	176	180	336	-22	0
3	4	0	707	0	843	-39	0	1006	180	180
2	5	0	630	180	448	-122	180	887	-1	0
1	2	0	584	0	721	-6	0	1131	169	180
4	2	0	560	180	281	165	180	251	-137	180
3	3	0	533	0	525	-36	0	475	5	0
2	2	0	459	180	690	163	180	866	180	180
3	1	0	440	180	481	37	0	547	-33	0
1	5	0	439	0	431	-19	0	332	-38	0
1	6	0	416	0	242	36	0	304	-117	180
2	0	0	396	0	755	-164	180	-	-	-
4	1	0	392	180	312	179	180	186	45	0
3	2	0	258	180	-	-	-	-	-	-
0	2	0	236	180	721	-115	180	-	-	-
2	4	0	215	180	831	-178	180	406	119	180
2	3	0	193	180	636	5	0	436	126	180
1	3	0	192	180	1054	-1	0	745	-3	0
0	4	0	177	180	612	-175	180	-	-	-
1	1	0	147	180	1165	180	180	788	-138	180
1	4	0	123	180	308	-114	180	372	3	0
2	1	0	89	180	255	-38	180	360	-39	0

Among all the 33 reflections up to 1.6 Å, the strongest one is (0 6 0). This reflection generates a cosine wave which cuts the *a* axis zero times per unit cell and the *b* axis 6 times. It is the phase of each reflection which determines where the maximum and minimum of the cosine wave are. The phase of (0 6 0) is 180^o (Table 1) and thus $\cos 180^o = -1$, the contribution to the potential at the origin is negative (black) (Fig. 1a). Similarly, the cosine wave given by (4 0 0) reflection cuts the *a* axis 4 times and the *b* axis zero times. The phase of (4 0 0) is also 180^o so its contribution to the potential at the origin is also negative (Fig. 1b). The summation of these two cosine waves is shown in Fig. 1c.

The cosine waves generated by the second strongest reflection (3 5 0) and its symmetry-related reflection (3 -5 0) are shown in Figs. 1d and e. Both cosine waves cut the *a* axis 3 times per unit cell and the *b* axis 5 times, however, they are oriented differently. The summation of the two symmetry-related cosine waves is shown in Fig. 1f).

When the 4 strongest independent reflections (in total 6 reflections including symmetry-related ones) are added, the map already shows some indication of where the atoms should be located within the unit cell (Fig. 1g). After the strongest 1/3 (11) of all the independent reflections has been included, all the atoms appear in the map (as white dots) (Fig. 1h). The map generated from all the 33 unique reflections (Fig. 1i) is only slightly better, because the 22 reflections further added in are weaker and so do not contribute very much to the Fourier map. The weak reflections are, however, equally important as the strong ones in the last step of a structure determination, the refinement.

In summary, as along as the crystallographic structure factor phases of the strongest reflections are correct, the reconstructed map represents the true (projected) potential distribution of the crystal. Once the potential distribution of the crystal is available, atomic positions can immediately be determined from the peaks of high potential in the map. Thus ***to determine crystal structures is equivalent to determine crystallographic structure factors.***

4. PHASES IN HREM IMAGES

Electron crystallography provides two major advantages over X-ray crystallography for determination of atomic positions in crystal structures; extremely small samples can be analysed and the crystallographic structure factor phases can be determined from images[21]. The crystallographic structure factor phases must be known in order to arrive at a structure model,

but these phases cannot be measured experimentally from diffraction patterns.

It is the *raison d'être* of electron microscopy that the phase information is preserved in the EM images, such that they represent a magnified image of the object. DeRosier and Klug[21] recognised that the crystallographic structure factor phases could be extracted directly from the Fourier transforms of digitised images, under the assumption of weak scattering and linear imaging, i.e. for very thin crystals. This discovery, for which Klug was awarded the Nobel Prize in Chemistry in 1982, can be considered as the birth of structure determination from HREM images.

5. HREM IMAGES AND PROJECTED POTENTIAL

The relation between an HREM image and the projected crystal potential is quite complex if the crystal is thick. To obtain an image which can be directly interpreted in terms of projected potential, crystals have to be well aligned, thin enough to be close to weak-phase-objects and the defocus value for the objective lens should be optimal, i.e. at the Scherzer defocus.

For a weak-phase-object, the Fourier transform of the HREM image $I_{im}(\mathbf{u})$ is related to the structure factor $F(\mathbf{u})$ by[22]:

$$I_{im}(\mathbf{u}) = \delta(\mathbf{u}) + k'T(\mathbf{u})\mathbf{F}(\mathbf{u}) \tag{3}$$

where k' is a constant and $T(\mathbf{u})$ is called the contrast transfer function (CTF). The effects of the contrast transfer function will be discussed in section 8.

For an image taken at Scherzer defocus, where $T(\mathbf{u}) \approx -1$ over a large range of resolution, the structure factor $F(\mathbf{u})$ can be obtained from the Fourier transform of the HREM image $I_{im}(\mathbf{u})$:

$$F(u) \approx -\frac{1}{k'} I_{im}(u) = \frac{1}{k'} \exp(\mathbf{i}\pi) I_{im}(u) \tag{4}$$

After fixing the unit cell origin (see section 10), the amplitudes and phases of the crystallographic structure factors are proportional to the amplitudes and phases of the corresponding Fourier components of the Fourier transform $I_{im}(\mathbf{u})$ of the image. All the phases in the Fourier transform $I_{im}(\mathbf{u})$ of the image, within the Scherzer resolution limit are shifted by 180° from the structure factor phases.

The projected potential can be obtained from the Fourier transform $I_{im}(\mathbf{u})$ of the image:

$$V(\mathbf{r}) \approx \frac{-1}{k'} \sum_{\mathbf{u}} I_{im}(\mathbf{u}) \exp\left[-2\pi i(\mathbf{u}\cdot\mathbf{r})\right] = -\frac{I_{im}(\mathbf{r})}{k'} \qquad (5)$$

The projected potential is proportional to the negative of the image intensity, i.e. black features in HREM positives (low intensity) correspond to atoms (high potential). The corresponding image is called the structure image.

Accurate atomic coordinates can be determined from the HREM images, with the help of crystallographic image processing. The experimental procedures for structure solution of inorganic crystals by HREM and crystallographic image processing are summarized in Figure 2.

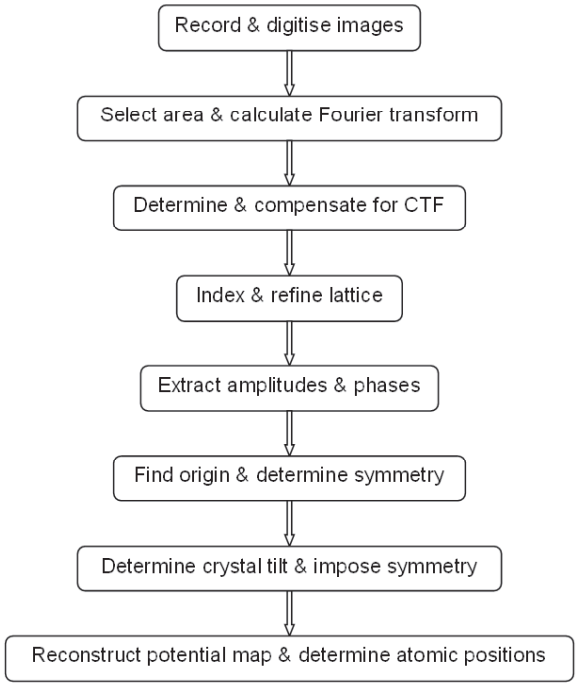

Figure 2 Flow diagram of structure determination by crystallographic image processing.

6. RECORDING AND QUANTIFICATION

Taking good HREM images is a critical step of any structure determination. The thinnest parts of the crystals should be used, to avoid strong multiple scattering. Only then are we close to the kinematical condition, where the relation between the amplitudes and phases extracted

from HREM images and the structure factor amplitudes and phases is simple.

Whenever possible, an amorphous area at the edge of the crystal should be included in the HREM images when images are recorded. This will help in the determination of the contrast transfer function. A set of images with different defocus values should be recorded, although it is often possible to solve structures from just a single image. The reasons will be described in section 9.

HREM images can be recorded on different media, such as photographic films, video rate CCD-cameras, slow-scan CCD cameras and image plates. For on-line digitisation, slow-scan CCD cameras provide good linear response and large dynamical range, but cover a smaller area than photographic films. On the other hand, image plates combine the large view area of the photographic films with the good linear response of the slow scan CCD cameras. However, both instruments are expensive. For off-line digitisation of photographic films, microdensitometers, slow-scan CCD cameras, video rate CCD-cameras and scanners can be used.

It is important to choose a suitable sampling size of the image, i.e. number of Ångströms per pixel. Each sampling pixel should be about 2-3 times smaller than the image resolution so as to preserve the high resolution information of the image. On the other hand, the grey-level linearity of the instruments for digitising is not very critical for determination of atom positions. Images can be digitised from both positives and negatives, using any digitising instruments, as long as the density values of the image are not saturated.

7. AMPLITUDES AND PHASES FROM IMAGES

Theoretically, HREM images of a weak-phase-object taken at Scherzer defocus represent directly the projected potential to a certain resolution (which may or may not be sufficient to reveal all the structure features of interest). However, in practice there are additional problems. Features in different unit cells are slightly different and symmetry-related features in the same unit cell are not exactly identical as they should be, as seen in Fig. 2. Lattice averaging over all the unit cells can be applied to produce an average structure. A further improvement can be reached by crystallographic image processing, imposing the crystallographic symmetry of the projection. These two steps are performed in reciprocal space. The different steps involved in solving an unknown crystal structure from HREM images and the refinement against SAED data will be outlined in the rest of the chapter, using several inorganic structures as examples; Ti_2S[26], $K_7Nb_{15}W_{13}O_{80}$[16],

$K_2O{\cdot}7Nb_2O_5$[27] and $Ti_{11}Se_4$[12]. The crystallographic image processing was carried out with the computer program CRISP[28], which has been designed especially for electron crystallography.

Figure 3a shows an HREM image of Ti_2S crystal taken along the short *c* axis. This image is first digitised and the thinnest area is selected from the image. The Fourier transform (FT) from this thinnest area is calculated. The image density is a set of real numbers, while the Fourier transform of the image is a set of complex numbers which can be expressed as an amplitude part and a phase part. The amplitude part of the FT is shown in Fig. 3b.

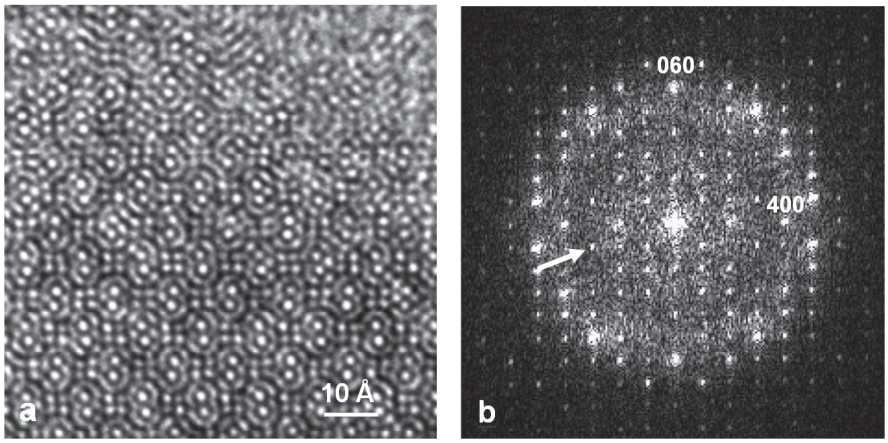

Figure 3 (a) HREM image of Ti_2S along the c axis taken on a Philips CM30/ST microscope at 300kV. (b) The Fourier transform of the image in (a). The dark ring in the FT, corresponding to the first crossover of the contrast transfer function, is indicated by an arrow.

The crystal structure information is periodic in the image and thus is concentrated at discrete diffraction spots in the FT. The amplitude and phase part of the FT around one such diffraction spot is shown in Fig. 4. The lattice in the FT is refined using all spots and the exact position of each reflection is predicted from the refined lattice. Integrated amplitudes and phases for all reflections are extracted from the numerical data around the expected center of the diffraction spots[28].

Digital Map of FFT

Ampl	40	41	42	43	44	45	46	47	48
-67	24	37	19	25	68	55	25	3	16
-66	30	74	41	77	73	38	27	44	32
-65	54	41	94	50	29	50	100	19	27
-64	88	100	77	191	69	139	40	80	50
-63	45	136	58	152	771	185	177	129	49
-62	52	84	164	326	1588	666	262	102	38
-61	87	54	100	60	930	382	243	72	36
-60	64	53	120	161	122	122	106	113	66
-59	34	64	152	32	157	47	99	43	48
-58	58	44	46	54	104	64	68	19	3
-57	31	86	69	61	60	94	80	31	44
Phas	**40**	**41**	**42**	**43**	**44**	**45**	**46**	**47**	**48**
-67	45	-155	98	165	123	136	140	-96	111
-66	-95	76	16	-108	-93	-126	93	2	141
-65	79	-30	-148	135	100	147	125	-3	53
-64	-24	-179	147	-42	-49	-64	22	82	-81
-63	-101	101	-56	175	91	93	-117	38	-180
-62	-71	-1	-108	58	32	16	-161	-17	80
-61	-149	-139	-170	18	-22	-43	135	-21	75
-60	127	137	-40	97	72	93	35	-54	54
-59	22	100	-113	-98	27	55	-155	-126	21
-58	-77	-27	47	154	-145	-178	77	-2	54
-57	-162	-151	-52	-22	-142	-127	-61	142	129

Figure 4 Extraction of amplitudes and phases from the Fourier transform of the image. Amplitudes and phases around the reflection (3 5 0) at pixel position (44 -62) in the FT are shown in digits. The amplitude for reflection (3 5 0) is extracted by first integration of 3x3 pixels around position (44 -62) and then subtraction of the averaged background estimated around the diffraction spot. The phase for reflection (3 5 0) is the phase value at the position (44 -62) i.e. 32°.

If an inverse Fourier transform is calculated using the amplitudes and phases extracted from the FT for all the reflections, a lattice averaged map with *p1* symmetry is obtained (Fig. 5a). This map is not yet proportional to the projected potential. The various distortions introduced by the electron-optical lenses, crystal tilt etc. must first be corrected for.

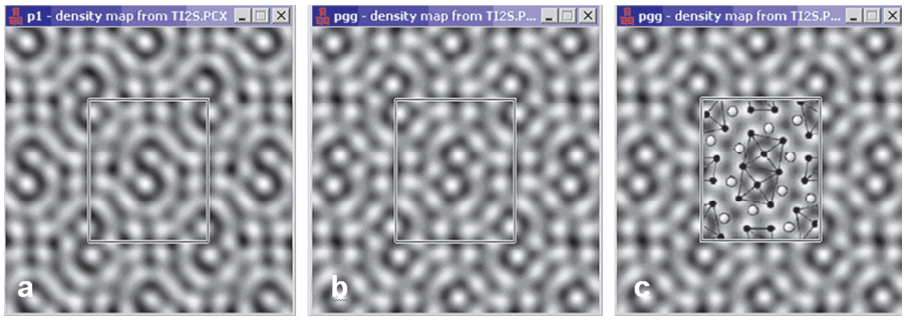

Figure 5 (a) The lattice averaged map of Ti_2S with *p1* symmetry, obtained by inverse Fourier transformation of the amplitudes and phases of all reflections extracted from the FT of the image. (b) The projected potential map reconstructed from the image after compensating for the contrast transfer function and imposing the crystal symmetry *pgg*. (c) The structure model is deduced from the reconstructed potential map (b) and superimposed on (b). The 24 strongest peaks (of which 6 are unique) in the unit cell are assigned to Ti atoms (in solid circles), which form octahedral clusters. The 12 weaker peaks (two unique) are S atoms (marked by open circles).

8. CORRECTING DEFOCUS AND ASTIGMATISM

As mentioned in section 6, the structure factors F(**u**) are proportional to the Fourier components $I_{im}(\mathbf{u})$ of the HREM image and the projected potential is proportional to the negative of the image intensity, if the image is taken Scherzer defocus where the contrast transfer function T(**u**) ≈ -1. In general, the Fourier components $I_{im}(\mathbf{u})$ are proportional to the structure factors F(**u**) multiplied by the contrast transfer function (CTF). The contrast transfer function $T(\mathbf{u}) = D(\mathbf{u})\sin\chi(\mathbf{u})$ is not a linear function. It contains two parts[29]: an envelope part D(**u**) which dampens the amplitudes of the high resolution components:

$$D(\mathbf{u})=\exp[-\tfrac{1}{2}\pi^2\Delta^2\lambda^2\mathbf{u}^4]\exp[-\pi^2\alpha^2\mathbf{u}^2(\varepsilon+C_s\lambda^2\mathbf{u}^2)^2] \quad (6)$$

and an oscillating part sinχ(**u**) which determines the contrast of the image, where

$$\chi(\mathbf{u}) = \pi\varepsilon\lambda\mathbf{u}^2 + \frac{\pi C_s\lambda^3\mathbf{u}^4}{2} \quad (7)$$

ε is the defocus value, C_s the spherical aberration constant, Δ the focus spread and α the electron beam convergence.

The objective lens transfers different structure factors F(**u**) into the HREM image in different ways, depending on the value of the contrast transfer function $D(\mathbf{u})\sin\chi(\mathbf{u})$. Phases of the Fourier components $I_{im}(\mathbf{u})$ of the image are related to the phases of the structure factors in the following way: those Fourier components in the range where sinχ(**u**) > 0 will have the same phases as the phases of structure factors, giving rise to the same contrast in the image as the projected potential; those Fourier components in the range where sinχ(**u**) < 0 suffer a phase change of 180°, giving a reversed contrast in the image. As a result, an HREM image is usually formed by the combination of Fourier components with both correct and inverted phases with respect to the structure factors.

Amplitudes of the structure factors are sampled by $|D(\mathbf{u})\sin\chi(\mathbf{u})|$ when they are transferred to the image. The most significant effect of the lens to the amplitudes is caused by the $|\sin\chi(\mathbf{u})|$ part, which oscillates with **u**. Reflections in the resolution regions where $|\sin\chi(\mathbf{u})| \approx 1$ are maximally transferred by the lens, while those at resolutions where $\sin\chi(\mathbf{u}) \approx 0$ are not transferred at all. This can be seen in the Fourier transform of HREM images from amorphous materials (Fig. 6), where the highest amplitudes (brightest areas) correspond to $|\sin\chi(\mathbf{u})| \approx 1$, while the lowest amplitudes (darkest areas) correspond to $|\sin\chi(\mathbf{u})| \approx 0$. If there is no astigmatism in the objective lens, a

set of alternating bright and dark rings may be found in the FT of the image (Fig. 6b). If there is astigmatism, these rings become a set of ellipses (Fig. 6c) or in more severe cases hyperbolas (Fig. 6d).

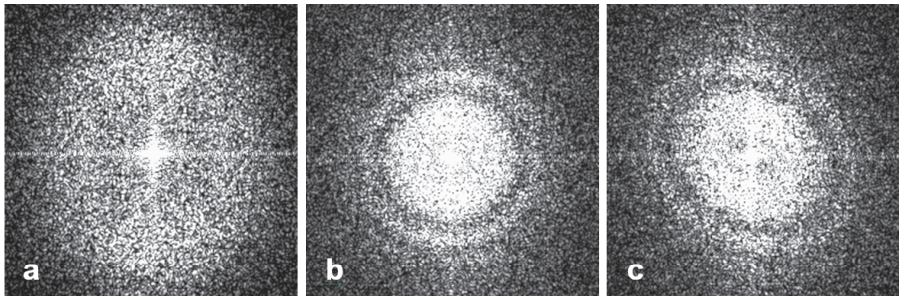

Figure 6 Fourier transforms of HREM images from amorphous carbon films taken (a) near Scherzer defocus, (b) at non-Scherzer without astigmatism and (c) with astigmatism.

In general, an image is a complicated mixture of structure factors which have been sampled by the contrast transfer function; some giving correct contrast and some giving reversed contrast. In summary, the contrast transfer function T(**u**) is strongly affected by the defocus value and astigmatism, resulting in drastic contrast changes in HREM images.

The defocus value can be determined experimentally from HREM images, using different methods[30, 31, 32, 33]. Here we will use a method similar to that used by Erickson and Klug[30] and Krivanek[31] to determine the defocus and astigmatism from the amorphous region of the image. This will be demonstrated first on the HREM image of Ti_2S (Fig. 3) which was taken with very little astigmatism and then on an image of $K_7Nb_{15}W_{13}O_{80}$[16] (Fig. 8) which is more astigmatic.

In the Fourier transform (FT) of an image containing both crystalline and amorphous regions, the sharp diffraction spots come from the periodic features, while the diffuse background in the FT comes from the amorphous region, as seen in Figs. 3b and 8b. The effects of the CTF are visible in the diffuse background of the FT, seen mostly as dark rings which correspond to where $\sin\chi(\mathbf{u}) \approx 0$.

The u values at the dark rings can be read out from the Fourier transform of the images where

$$\chi(\mathrm{u}) = \pi\varepsilon\lambda\,\mathrm{u}^2 + \frac{\pi C_s \lambda^3\,\mathrm{u}^4}{2} = \mathrm{n}\,\pi \qquad (8)$$

and $n = 0, \pm1, \pm2, \ldots$ are integers. In general, the first crossover corresponds to $\chi(\mathbf{u}) = 0$ (n = 0) if the defocus is near zero, $\chi(\mathbf{u}) = -\pi$ (n = -1) for

underfocus and $\chi(\mathbf{u}) = \pi$ (n =1) for overfocus. If both λ and C_s are known, the defocus value ε can be determined from the position of the first crossover by:

$$\varepsilon = \frac{n}{\lambda u^2} - \frac{C_s \lambda^2}{2} u^2 \qquad n = 0, \pm 1 \qquad (9)$$

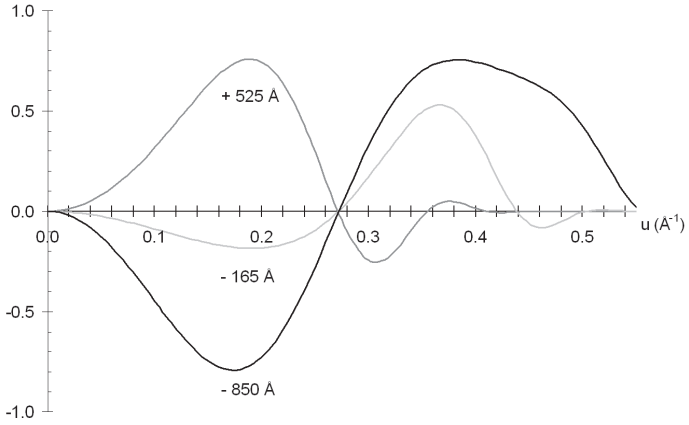

Figure 7 Contrast transfer functions T(u) at defocus values ε = -850 Å, -165Å and -525Å. The optical parameters are from a Philips CM30/ST microscope: U = 300 kV, C_s=1.15 mm, Δ = 70 Å and α = 1.2 mrad. All the three contrast functions have a common first crossover position at u = 0.272 Å^{-1}. The defocus value -850 Å was determined to be the correct defocus for the image of Ti_2S shown in Fig. 2.

Different values of n give different solutions for the defocus. For example, the HREM image of Ti_2S shown in Fig. 3a was taken on a Philips CM30/ST microscope operated at 300 kV. The electron wavelength λ is 0.197 Å and the spherical aberration constant C_s is 1.15 mm. The first crossover is determined at u = 0.272 Å^{-1} from the Fourier transform of the image (Fig. 3b). Three possible defocus values, -165 Å (n = -1), -850 Å (n = 0) and +525 Å (n = 1), are deduced from Eq. 9, all giving a first crossover at u = 0.272 Å^{-1}. The corresponding contrast transfer functions at these three defocus values are shown in Fig. 7. The value -850 Å is chosen to be the correct defocus since the calculated CTF at this defocus gives the best fit to the intensity distribution of both the diffraction spots and the background noise in the FT of the image (Fig. 3b). The CTF at the defocus -165 Å would result in much too low amplitudes at low resolution while that at the defocus 525 Å would give much too low amplitudes in the high resolution range, which do not agree with the FT of the image (Fig. 3b). The decision of which of the three possible defocus values is correct can also be based on the positions of the second and third zero crossovers, if visible in the FT [16].

For an image such as that of $K_7Nb_{15}W_{13}O_{80}$ along the *c* axis shown in Fig. 8a, the Fourier transform (Fig. 8b) shows a dark elliptical ring together with the diffraction spots. This implies that the defocus values are different along different directions in the Fourier transform. First the defocus values $\varepsilon_{\underline{u}}$ and $\varepsilon_{\underline{v}}$ along the minor and major axes of the ellipse (or hyperbola) are determined from the positions of the first crossovers along the minor and major axes of the ellipse. Then the defocus value along any arbitrary direction in the FT is deduced by

$$\varepsilon(\theta) = \varepsilon_{\underline{u}} \cos^2(\theta) + \varepsilon_{\underline{v}} \sin^2(\theta) \tag{10}$$

where θ is the angle between the direction and the minor axis. The corresponding contrast transfer function $T(\mathbf{u})=D(\mathbf{u})\sin\chi(\mathbf{u})$ along this direction can be calculated. Two contrast transfer functions at defocus values -1321 Å and -947 Å along the minor and major axes of the ellipse, determined from the FT of the image (Fig. 8b) are shown in Fig. 8d.

Mathematical CTF correction: calculating first the mathematical contrast transfer function $T(\mathbf{u})$ from the estimated defocus values. Then the structure factor is calculated from the Fourier transform $I_{im}(\mathbf{u})$ of the image for all $\mathbf{u}$ except those with $\sin\chi(\mathbf{u}) \approx 0$ by:

$$F(u) = \frac{1}{k'} \cdot \frac{I_{im}(u)}{T(u)} \tag{11}$$

The projected potential of the crystal can be calculated by inverse Fourier transformation:

$$V(\mathbf{r}) = \frac{1}{k'} \sum_{\mathbf{u}} \left\{ \frac{I_{im}(\mathbf{u})}{T(\mathbf{u})} \exp\left[-2\pi i(\mathbf{u}\cdot\mathbf{r})\right] \right\} \tag{12}$$

The potential map obtained after the CTF correction (Fig. 8f) can be readily interpreted in terms of atomic structures while the map before the CTF correction and imposing the symmetry (Fig. 8e)

In most cases it is possible to retrieve the projected potential map from a single image taken under non-optimal conditions[16, 34]. However, the structure factors can be determined more accurately and an even more accurate potential projection can be obtained by combining a series of through-focus images[16]. Information contributed by kinematical scattering can be maximally extracted and the non-linear effects minimized by combining a series of through-focus images. Thus the structure can be determined more accurately and reliably[18, 35, 36].

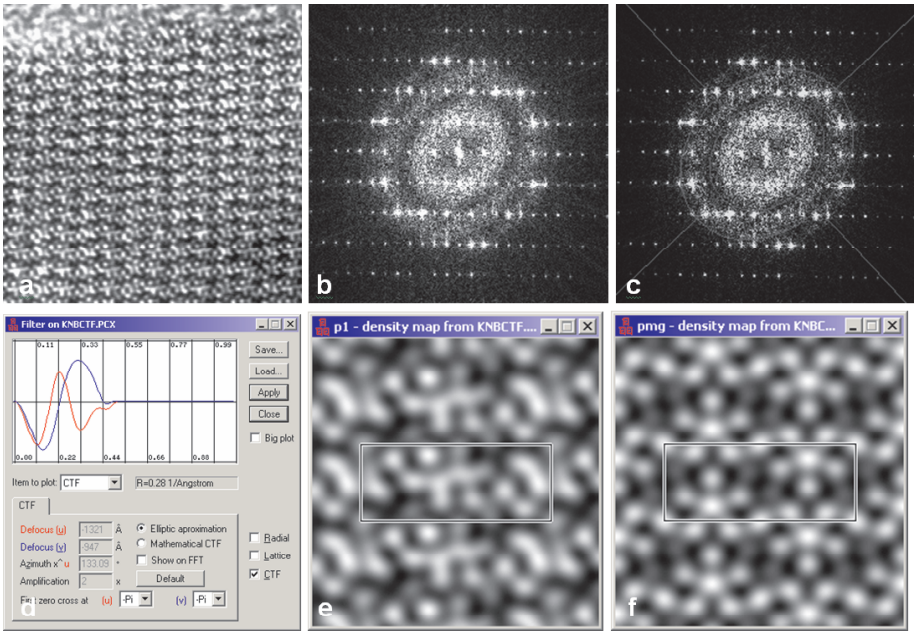

Figure 8 (a) HREM image of $K_7Nb_{15}W_{13}O_{80}$ along the c axis taken at non-Scherzer defocus[16]. (b) The Fourier transform of $I_{im}(u)$ of the image in (a). An elliptic dark ring can be seen in the background noise of the FT, which correspond to the first crossover of the CTF. (c) A set of ellipses are fitted to the dark rings. (After Zou et al. [16]) (d) The defocus values along the minor and major axes are estimated from the innermost ellipse to be -1321 and -947 Å. The two corresponding CTF curves are shown. (e) The lattice averaged map $K_7Nb_{15}W_{13}O_{80}$ obtained from the image in (a). (f) the projected potential map reconstructed from (a) after compensating for the CTF and astigmatism and imposing the crystal symmetry *pmg*.

9. SYMMETRY DETERMINATION

Symmetry can be determined by different methods. In X-ray crystallography, the symmetry determination is carried out using symmetry-relations of amplitudes combined with systematic absences. In electron diffraction and HREM images, due to multiple scattering, symmetry forbidden reflections are often not absent. Since the systematic absences are often unreliable in electron crystallography experiments, amplitude relations alone are often not sufficient for differentiating between different symmetries. However, the phases, experimentally observed in HREM images, have much better quality and can be used for symmetry determination.

The quality of the measured phases can be characterised by the averaged phase error (phase residual ϕ_{Res}) of symmetry-related reflections:

$$\phi_{Res} = \frac{\sum_{h\,k}\left[w(h\,k)\left|\phi_{obs}(h\,k) - \phi_{sym}(h\,k)\right|\right]}{\sum_{h\,k} w(h\,k)} \qquad (13)$$

where w($h\ k$) is a weighting factor given to the reflection ($h\ k$) (usually set to be equal to the amplitude of the reflection ($h\ k$)), ϕ_{obs} ($h\ k$) is the experimentally observed phase and ϕ_{sym} ($h\ k$) is the phase which fulfils the symmetry relations and restrictions. The phase relations and phase restrictions are different in each of the 17 plane groups These relations are tabulated and listed for example in Table 3.1 in Zou[18](1995)

Unlike amplitudes, phases are not absolute values, but relative to an origin. When the Fourier transform of an image is calculated, the origin is at an arbitrary position in the unit cell. Phases do not have to obey the phase relations and restrictions, and thus the phase residual ϕ_{Res} is large. The points in the unit cell which have the same relations to the symmetry elements as the origin specified in the International Table for Crystallography is located as described below (for example in centrosymmetric plane groups, the origin should coincide with a center of symmetry). The origin is shifted 360° by 360° in small steps over the entire unit cell and at each step the phase residual ϕ_{Res} is calculated. When all positions are tested within the unit cell, the position ($x_0\ y_0$) which gives the lowest phase residual ϕ^0_{Res} is considered to be the correct origin. Finally all phases are recalculated relative to this origin. This procedure is known as origin refinement.

The symmetrized phase ϕ_{sym} ($h\ k$) is estimated from the experimental phases ϕ_{obs} ($h\ k$) as follows:

- If a reflection ($h\ k$) is not related to other reflections by the symmetry (except by Friedel's law):

$$\phi_{sym}(h\,k) = \phi_{obs}(h\,k) \qquad (14)$$

- If a reflection ($h\ k$) is symmetry-related to other reflections, the phases for this group of reflections are judged together. ϕ_{sym}($h\ k$) is determined by vector summation of all these reflections:

$$\phi_{sym}(h\,k) = tan^{-1}\left[\frac{\sum_j w^j s^j \sin\left(\phi^j_{obs}(h\,k)\right)}{\sum_j w^j s^j \cos\left(\phi^j_{obs}(h\,k)\right)}\right] + \begin{cases} 0^\circ & \left[\text{if } \sum_j w^j s^j \cos\left(\phi^j_{obs}(h\,k)\right) > 0\right] \\ 180^\circ & \left[\text{if } \sum_j w^j s^j \cos\left(\phi^j_{obs}(h\,k)\right) < 0\right] \end{cases} \quad (15)$$

where the summation is for all symmetry-related reflections in the group (including the (h k) reflection). w^j is a weighting factor which can be set either to 1 or for example to the amplitude $\left|F^j_{obs}(h\,k)\right|$ of the corresponding reflection. $s^j = 1$ if the phases $\phi_{sym}(h\,k)$ and $\phi^j_{obs}(\mathrm{h\,k})$ should be equal and $s^j = -1$ if they should differ by 180°.

- For centrosymmetric projections, $\phi_{sym}(h\,k)$ is finally set to 0° if $-90° < \phi_{sym}(h\,k) < 90°$, otherwise it is set to 180°.

Each symmetry has a unique set of phase relations and phase restrictions. Thus, the phase residuals calculated for an image will be different for different symmetries. Once the phase residuals for each of the 17 plane group symmetries have been calculated, the projected symmetry (plane group) of the crystal can be deduced by comparing these phase residuals. Usually the symmetry with the lowest phase residual is the correct symmetry. If phase residuals for several plane groups are similar, the highest symmetry is normally chosen.

The procedure of symmetry determination is demonstrated (Fig. 9) for the [001] projection of Ti_2S, by analysing phases extracted from the HREM image shown in Fig. 3a. Since the lattice of Ti_2S is primitive and the cell dimensions *a* and *b* are not equal, the possible plane groups are *p1*, *p2*, *pm*, *pg*, *pmm, pmg* and *pgg*. Among those 7 possible plane groups, *p2*, *pg* and *pgg* give relatively low phase residuals (12.5º, 7.7º and 11.3º, respectively). The symmetry of the projection is most probably *pgg*, according to the criteria mentioned above. Notice that the two lower symmetries *p2* and *pg* are subgroups of *pgg*.

In the plane group *pgg* phase restrictions and phase relations for all reflections (once the origin has been shifted to a point with the same relation to the symmetry element in the unit cell as specified in the Int. Table for Crystallography) are: all phases have to be 0º or 180º and phases of all

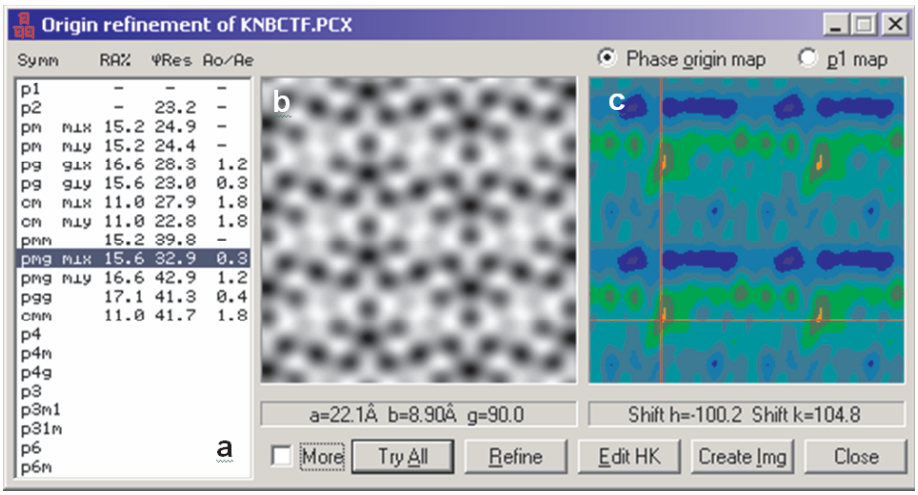

Figure 9 Symmetry determination and origin refinement of $K_7Nb_{15}W_{13}O_{80}$. a) The crystallographic R-value on symmetry-related reflections R_{sym} (here called RA%) is similar for all these plane groups, because they all have the same mm-symmetry relations of amplitudes. In contrast, the phase residual ϕ_{Res} is different in different plane groups and thus can be used to determine the symmetry. b) the map after imposing the symmetry *pmg*. c) Phase residual map showing how ϕ_{Res} varies when the origin is shifted throughout one unit cell. The lowest value of ϕ_{Res} is found at position (-100.2°/360°, 104.8°/360°), so that the position is chosen as the phase origin.

symmetry-related pairs (*h k*) and (-*h k*) are related by $\phi(h\ k) = \phi(-h\ k) + (h + k)\cdot 180°$[18]. Furthermore, all symmetry-related pairs *(h k)* and (-*h k*) should have the same amplitude. After the symmetry *pgg* has been imposed to the amplitudes and phases (see Table 1), the inverse Fourier transform gives a density map (Fig. 5b and 1*l*) which is quite similar to the projected potential map shown in Fig. 1k.

10. INTERPRETATION OF PROJECTED POTENTIAL MAPS

The projected potential map obtained from HREM images after image processing must now be interpreted in terms of chemical structure. At this stage it is of great value to be familiar with the chemical system under investigation. Only in the most fortunate cases there is a one-to one correspondence between the peaks in the map and atoms in the structure. In the many cases where the structure consists of two or more atomic species with very different scattering factors, the lighter atoms are often not seen at

all. The resolution is also an important factor here; the interatomic distances in metal oxides are often about 2 Å for metal-oxygen and 4 Å for metal-metal. Thus, at 2.5 Å resolution we may expect to see peaks corresponding to MeO_n polyhedra, but we should not expect to see resolved oxygen atoms. This is the situation for the metal oxides presented in this chapter. For Ti_2S the situation is better; Ti and S are about equally large and sufficiently well separated so that the 1.9 Å resolution of the images in Fig. 5b, is sufficient to resolve all atoms. Atomic positions can be determined directly from the peaks (white spots) in this density map.

In most cases the chemical composition, unit cell dimensions and symmetry are known. We can then estimate the number of formula units in the unit cell from the fact that each atom (except hydrogen) occupies about 15 - 20 $Å^3$. If the HREM image is taken along a short unit cell axis (< 5 Å), the whole structure may be resolved in that single projection.

Unfortunately, HREM images are black and white only, so there is no direct evidence of which peaks correspond to which atom species. In principle we might expect the heights of the peaks to be proportional to the scattering power of the atoms, but this is not always the case, due to the relatively poor quality of the amplitudes in HREM images. Here again chemical knowledge is indispensable. In the case of Ti_2S, it is known that the Ti atoms often arrange in octahedral clusters, while the S atoms prefer to be inside trigonal bipyramids. With this chemical background, the peaks in the potential map (Fig. 5b) can easily be assigned to Ti or S, as shown in Fig. 5c.

11. CRYSTAL THICKNESS AND CRYSTAL TILT

Crystal tilt is one of the main reasons why HREM images often cannot be directly interpreted in terms of projected crystal structure. The alignment of the crystal in the microscope is usually judged from the SAED pattern, which comes from an area much larger than the area selected for image processing. Even if the SAED pattern is well aligned, the thin area of the crystal selected for image processing may still be slightly tilted if the crystal is bent. An HREM image from a slightly misaligned crystal is similar to the image from a thinner and well aligned crystal. This indicates that the weak-phase-object approximation will be valid for an even thicker crystal if the crystal is a slight crystal tilt [37,38]. This also causes that the crystal thickness estimated by image matching using image simulation are often smaller than the true value[37].

The main effect of crystal tilt is to smear out the structural information in the direction perpendicular to the tilt axis. Atoms from different unit cells no longer project exactly on top of each other. The projection of an atom

column becomes a line rather than a point. This smearing is equivalent to loosing the fine details in the direction perpendicular to the tilt axis. As a consequence, the symmetry of the crystal is often lost in the images (Fig. 10b); the amplitudes of reflections away from the tilt axis are attenuated (Fig. 10d). The effect of crystal tilt depends on the crystal thickness; the thicker the crystal, the more rapidly $I_{im}(\mathbf{u})$ is attenuated. The overall effect of crystal tilt on the image is given by the product of the crystal thickness t and the tilt angle γ, $t \cdot \sin\gamma$[18]. Even for the smallest tilts and thinnest crystals, the effect on amplitudes is significant. Pairs of symmetry-related reflections no longer have the same amplitudes if one of the reflections is close to the tilt axis and the other further away.

Furthermore, the effect of crystal tilt on a specific reflection depends on the distance of that reflection to the tilt axis. If the reflection lies on the tilt axis, it will not be affected by crystal tilt. The further away the reflection is from the tilt axis, the more attenuated is $I_{im}(\mathbf{u})$. The thickness of the crystal can be determined directly from the image, if images from at least two different crystal tilts are recorded, as described by Hovmöller and Zou[27].

The effects of crystal tilt on phases is quite different. The phases are practically unaffected for small tilts and thin crystals[18]. However, as long as the product $t \cdot \sin\gamma$ is small, the phases are unchanged. Both phase relations and phase restrictions are still valid. Thus, it is possible to determine the (projected) crystal symmetry also from an image of a tilted crystal, using the phases.

For most thin crystals, the distortion of the image due to crystal tilt can be compensated by imposing the crystal symmetry on the amplitudes and phases extracted from the image.

The projected potential can be reconstructed. This reconstruction method is demonstrated in Fig. 10 on HREM images of $K_2O \cdot 7Nb_2O_5$. This method is especially powerful for crystals with high symmetries.

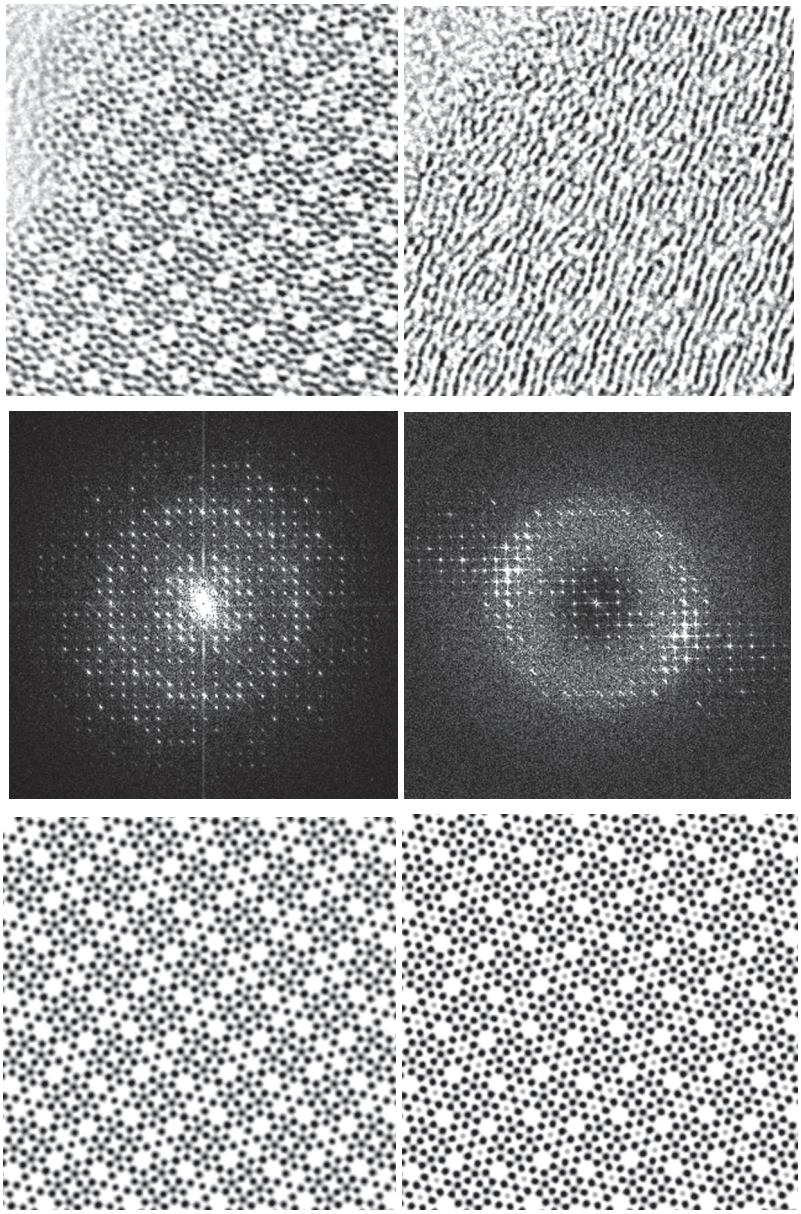

Figure 12 HREM images of K2O·7Nb2O5 along the c-axis from (a) a well-aligned crystal and (b) the same crystal tilted 5°. Atom columns which are separated in (a) are smeared out into lines perpendicular to the tilt axis. (c) and (d) The corresponding Fourier transforms of images (a) and (b). The tilt axis is indicated by a line in (d) and (e). Reflections further away from the tilt axis are attenuated. (e) and (f) Projected potential maps reconstructed by imposing the projection symmetry of the crystal, p4g, on the amplitudes and phases extracted from (c) and (d), respectively. The white dots in the maps are Nb atoms. The positions of the Nb atoms determined from both maps are very similar, within 0.02 Å.

12. CONCLUSIONS

It has been shown that crystal structures can be solved from HREM images. The experimental conditions defocus and sample thickness, which are only guessed in image simulation procedures, can be determined experimentally, as can also astigmatism and crystal tilt. Also the projected crystal symmetry can be determined. After correcting for the various distortions, a reconstructed projected potential map can be calculated. If the crystal is thin and the resolution of the electron microscope sufficiently high, this map will have peaks at the positions of the heaviest atoms. The structure can be confirmed and further improved by refinement, using SAED data to very high resolution.

Acknowledgements

This project was supported by the Swedish Research Council. XD Zou is a Research Fellow of the Royal Swedish Academy of Sciences supported by a grant from the Knut and Alice Wallenberg Foundation.

References

1. ZG Pinsker. Diffraktsiya elektronov (Izd-vo Akad. Nauk SSSR., Moscow 1949) [English transl,: Electron diffraction (Butterworths, London 1952)].
2. BK Vainshtein. Strukturnaya elektronographiya, Izd-vo Akad. Nauk SSSR., Moscow, 1956 [English transl,: Structure Analysis by Electron Diffraction. Pergamon Press Ltd., Oxford, 1964].
3. BK Vainshtein, BB Zvyagin, AS Avilov. Electron diffraction structure analysis, in Electron Diffraction Techniques, Vol. 1, J.M. Cowley, ed., Oxford Univ. Press, Oxford, 1992, pp. 216-312.
4. S Iijima. High resolution electron microscopy of crystal lattice of titanium-niobium oxide. J Appl Phys 42: 5891 - 5893, 1971.
5. MA O'Keefe, P Buseck, S Ijima. Computed crystal structure images for high resolution electron microscopy. Nature 274: 322 – 324, 1978.
6. PNT Unwin, R Henderson. Molecular structure determination by electron microscopy of unstained crystalline specimens. J Mol Biol 94: 425-440, 1975.
7. W Dong, T Baird, JR Fryer, CJ Gilmore, DD McNicol, G Bricogne, DJ Smith, MA O'Keefe, S Hovmöller. Electron microscope at 1 Å resolution by entropy maximization and likelihood ranking. Nature 355: 605-609, 1992.
8. S Hovmöller, A Sjögren, G Farrants, M Sundberg, B-O Marinder. Accurate atomic positions from electron microscopy. Nature 311: 238 – 241, 1984.

9. DN Wang, S Hovmöller, L Kihlborg, M Sundberg. Structure determination and correction for distortions in HREM by crystallographic image processing. Ultramicroscopy 25: 303-316, 1988.
10. JJ Hu, FH Li, HF Fan. Crystal structure determination of $K_2O{\cdot}7Nb_2O_5$ by combining high-resolution electron microscopy and electron diffraction. Ultramicroscopy 41: 387-397, 1992.
11. H-R Wenk, KH Downing, M Hu, MA O'Keeefe. 3D structure determination from electron-microscope images: electron crystallography of staurolite. Acta Cryst. A48: 700 -716, 1992.
12. T.E. Weirich, R. Ramlau, A. Simon, S. Hovmöller, X.D. Zou. A crystal structure determined to 0.02 Å accuracy by electron crystallography, Nature 382: 144-146, 1996.
13. J.M. Cowley. Diffraction Physics. 2nd edition, North-Holland, Amsterdam, 1984.
14. D.B. Williams, C.B. Carter. in Transmission Electron Microscopy. Vol. II, Plenum Press, New York, 1996, pp.203.
15. XD Zou. On the phase problem in electron microscopy: the relationship between structure factors, exit waves, and HREM images. Microsc. Res. Tech. 46: 202-219, 1999.
16. XD Zou, M Sundberg, M Larine, S Hovmöller. Structure projection retrieval by image processing of HREM images taken under non-optimum defocus conditions. Ultramicroscopy 62: 103-121, 1996.
17. D Van Dyck, M Op de Beeck. A simple intuitive theory for electron diffraction. Ultramicroscopy 64: 99 - 107, 1996.
18. XD Zou. Electron crystallography of inorganic structures - theory and practice. Chem. Comm. 5, Stockholm, Ph.D. thesis, 1995.
19. AL Patterson. A direct method for the determination of the components of interatomic distances in crystals. Z. Kristallogr. 90: 517 - 542, 1935.
20. JP Owens. BR Conrad, HF Franzen. The crystal structure of Ti_2S, Acta Cryst. 23: 77-82, 1967.
21. DL Dorset. Structural electron crystallography, Plenum Press, 1995.
22. XD Zou. Crystal Structure determination by crystallographic image processing. in "Electron Crystallography", eds. DL Dorset, S Hovmöller, XD Zou, Nato ASI Series C, Kluwer Academic Publishers, Dordrecht, 1997, pp163-181.
23. RVincent, PA Midgley. Double conical beam-rocking system for measurement of integrated electron diffraction intensities. Ultramicroscopy 53: 271 - 282, 1994.
24. XD Zou, Y Sukharev, S Hovmöller. ELD - a computer program system for extracting intensities from electron diffraction patterns. Ultramicroscopy 49: 147-158, 1993.
25. XD Zou, Y Sukharev, S Hovmöller., Quantitative measurement of intensities from electron diffraction patterns for structure determination - new features in the program system ELD. Ultramicroscopy 52: 436 - 444, 1993.
26. TE Weirich. Metallreiche systeme mit kondensierten clustern. Osnabrück University, Germany, Ph.D. thesis, 1996.
27. S Hovmöller, XD Zou. Measurement of crystal thickness and crystal tilt from HREM images and a way to correct for their effects. Microsco Res Tech 46: 147-159, 1999.
28. S Hovmöller. CRISP: crystallographic image processing on a personal computer. Ultramicroscopy 41: 121-135, 1992.
29. MA O'Keefe. "Resolution" in high-resolution electron microscopy. Ultramicroscopy 47: 282-297, 1992.
30. HP Erickson, A Klug. Measurement and compensation of defocusing and aberrations by Fourier processing of electron micrographs, Phil. Trans. Roy. Soc. Lond. B261: 105-118, 1971.

31. OL Krivanek. A method for determining the coefficient of spherical aberration from a single electron micrograph. Optik 45: 96-101, 1976.
32. FS Han, HF Fan, FH Li. Image processing in high-resolution electron microscopy using the direct method. II. Image deconvolution, Acta Cryst. A42: 353-356, 1986.
33. JJ Hu, FH Li. Maximum entropy image deconvolution in high resolution electron microscopy. Ultramicroscopy 35: 339-350, 1991.
34. A Klug. Image analysis and reconstruction in the electron microscopy of biological macromolecules. Chimica Scripta 14: 245 -256, 1978-79.
35. W Coene, G Janssen, M Op de Beeck, D Van Dyck. Phase retrieval through focus variation for ultra-resolution in field-emission transmission electron microscopy. Phys. Rev. Letts. 69: 3743-3746, 1992.
36. WO Saxton. What is the focus variation method? Is it new? Is it direct? Ultramicroscopy 55: 171-181, 1994.
37. MA O'Keefe, V Radmilovic. Specimen thickness is wrong in simulated HREM images. Proceedings of the 13th ICEM, Paris), Vol. 2B: 361-262, 1994.
38. XD Zou, EA Ferrow, S Hovmöller. Correcting for crystal tilt in HREM images of minerals: the case of orthopyroxene. Physics and Chemistry of Minerals 22: 517-523, 1995.